Wave-particle interactions in copper diamond

Marcus Portelli,[1] Michele Pasquali,[2] Federico Carra,[3] Alessandro Bertarelli,[3] Pierluigi Mollicone,[1] and Nicholas Sammut[1]

[1]*Abstract University of Malta, Msida 2080, Malta*
[2]*Sapienza University of Rome, Via Eudossiana 18, 00184 Rome, Italy*
[3]*CERN, Esplanade des Particules 1, 1211 Geneva 23, Switzerland*

(Received 11 May 2023; accepted 3 August 2023; published 31 August 2023)

In the context of wave propagation in solids caused by particle-matter interactions, the composite structure of copper diamond is believed to have a significant impact on the material's response. This limits the accuracy of isotropic homogeneous elastic and elastic-plastic models used in earlier studies modeling the material's behavior under such conditions. This study aims to investigate the mesoscopic behavior of the copper diamond and discusses the advantages and limitations of modeling the internal composite structure of the material. The material response of CuCD was modeled in a 2D finite element simulation, considering internal wave propagation as a result of external impact and an internal thermal shock. Various homogeneous models were considered and compared with a mesoscopic model. The homogeneous models tested were found to be able to capture wave propagation effects in the material, and the inclusion of a hardening model allowed their performance to approach that of the mesoscale model considered, which is significantly more computationally demanding.

DOI: 10.1103/PhysRevAccelBeams.26.084501

I. INTRODUCTION

The structure of many real, nonidealized media is quite complicated, and thus the idealization of such media as a homogeneous continuum is generally only valid up to a limiting scale of magnitude. Classical elasticity theory is typically applied to metals, which are polycrystalline on a microscale, i.e., they are made up of a number of randomly oriented anisotropic crystals. Similarly, material composites are comprised of a mixture of different materials with varying properties, leading to complex heterogeneity which sometimes cannot be accurately idealized as a homogeneous continuum.

Copper diamond (CuCD) is one such example of a composite material made up of a mixture of two constituents, namely diamond particles encased in a copper matrix. The material can thus either be described as a homogeneous medium, which is the case when testing for material properties using conventional tools such as the four-point bending test, or as a stochastic heterogeneous medium composed of a random distribution of diamond particles in copper. The diamond particles have thermomechanical properties which are significantly different from those of the surrounding material. The composition is similar to what is seen in plastic composites, where small spherical particles are commonly added to increase sound absorption and stiffness, and in spheroidized steel-carbide spheres in a ferrite matrix.

Wave propagation in stochastic media has been studied extensively by Sobczyk [1], who analyzed the behavior of elastic waves in stochastic solids, thermoelastic waves, as well as wave scattering at stochastic surfaces. Wave propagation in inhomogeneous media is intrinsically coupled with the phenomenon of scattering, which gives rise to a number of interesting physical effects such as wave attenuation, that is, the loss of energy of a propagating wave and the resulting reduction in the strength of the recorded signal. This phenomenon is similar to the dispersion of energy caused by wave distribution to a larger volume of material as it propagates cylindrically through a material. Most studies on the subject of wave propagation in stochastic media are based on various simplifications and assumptions of physical hypotheses, one such assumption being that the studied stochastic medium is only weakly inhomogeneous, i.e., fluctuations of properties are relatively small. This is not always the case, especially when characteristic lengths of the propagating wave, such as the wavelength, approach those of the material's inhomogeneities, as is the case for diamond particles in CuCD.

A. Copper diamond

CuCD is a novel composite material developed as a candidate for use in future collimators and absorbers being

implemented in the upcoming HL-LHC upgrade in CERN's LHC. CuCD is a metal-matrix composite (MMC), specifically a particle-reinforced metal-matrix composite (PRMMC), composed of a copper matrix with diamond particles dispersed in the material. The constituents are hot pressed in a spark plasma sintering process close to the melting temperature of copper. Several binding materials are added, including titanium, chromium, boron, zirconium, and titanium. In the sintering process, these additions form carbides that aid in bonding the diamond and copper particles, which otherwise have minimal chemical affinity [2]. The cost of diamond particles has decreased considerably with the advent of synthetic diamonds [3], making it possible to combine the stellar heat conduction of the material with the already high conductivity of copper. The conductivity of copper-diamond composites has consequently been studied extensively [4–8]. Alternative methods to the sintering process, which is expensive to conduct and requires precise control of various thermodynamic phenomena, have also been proposed, such as the electrodeposition of copper to synthetic diamonds [9].

Diamond has a very high thermal conductivity (approximately 2000 W/mK, a factor of 5 higher than that of copper). In contrast with metals, in which conduction is done via electrons, the high thermal conductivity of diamonds is a result of heat transfer by lattice vibrations. The copper-diamond interface plays an important role in the final CTE, thermal conductivity, and mechanical properties of the final composite, and the added binding materials promote the wetting and bonding of the diamond particles with the copper matrix. As mentioned, in diamonds, phonons dominate the heat conduction, while electrons dominate in copper. The thin interface layer formed by the carbide grade aids in the electron-phonon coupling and improves interfacial bonding, leading to an overlap in phonon densities of copper and diamond, which results in high thermal conductivities [10–12]. Best results are achieved by fast pressure-assisted sintering of powder mixtures, with an elevated heating and cooling rate (in the order of a 100 K/ min). This results in conductivities in the order of 640 W/mK in CuCD composites with carbide binders, compared to thermal conductivities in the order of 400 W/mK in composites with a pure copper matrix and no additional binders [13].

One of the CuCD grades tested in the MultiMat experiment, named CuCD RHP3434 for the scope of the experiment, was developed by RHP Technology [14]. The grade is primarily composed of synthetic diamond particles ($50\%_{vol}$) dispersed in a copper matrix ($50\%_{vol}$). Such a composition would result in a theoretical density of 6.2 g/cm^3; however, the actual density of the grade measures at 5.7 g/cm^3, indicating that the material has approximately $8.4\%_{vol}$ of porosity (i.e., the actual volume distribution is 8.4% porosities, 45.8% copper, and 45.8% diamond particles).

The grade is produced by a hot-pressing process (spark plasma sintering) using a compact of cold-pressed constituent powders, known as the "green". The green is composed of synthetic diamond particles, spheroidal copper, and additionally a small amount of amorphous boron as a binding element. These are sintered at pressures up to 35 MPa at a temperature slightly below the melting point of copper, approximately 1000–1050 °C. The process is conducted in a dry hydrogen gas atmosphere, and the pressure is maintained for 1–4 h, following which the setup is slowly cooled to 400 °C. A stress-relieving heat treatment is then conducted at temperatures of around 300–400 °C for another hour [15]. The carbide B_4C (boron carbide) is formed at the interface and provides a reliable bond between the copper and diamond particles.

The blend of properties provided by the two material constituents increasingly makes CuCD a material of interest in the field of beam intercepting devices (BIDs). While copper delivers good thermal and electrical conductivity, the diamond particles extend thermal conductivity further and help in lowering the coefficient of thermal expansion and density. CuCD has been chosen to replace Inermet180, a tungsten-heavy alloy, for use in the HL-LHC's tertiary collimators. Compared to Inermet180, CuCD is more robust and is able to tolerate higher beam intensities without succumbing to extreme damage and requiring replacement. Nevertheless, the material's limitations include the difficulty and cost of machining complex shapes with precise tolerances, along with the relatively high density and CTE compared to competing materials currently being developed at CERN, such as molybdenum graphite [16]. Another disadvantage of the material is the low melting point of the copper matrix and the fact that, due to the high copper content, the coefficient of thermal expansion increases significantly with temperature.

B. Wave propagation in BIDs

A number of characteristics have been identified to characterize the performance of BIDs. Along with general engineering requirements such as availability, cost, weight, and manufacturing feasibility, in the case of BIDs, other factors need to be considered such as resistance to high temperatures, mechanical robustness, resistance to radiation, (low) contribution to rf impedance, and geometrical stability.

Consequently, materials developed for and subject to these intense environments necessitate extensive experimental testing, allowing the derivation of constitutive models that can be used to replicate high-energy particle beam impacts in numerical simulations. CERN's HiRadMat (high radiation to materials) facility [17] was specifically designed with these kind of experiments in mind. Accelerator components and specimens can be tested in the HiRadMat facility, which delivers high-intensity beams to an irradiation area [18,19].

Full-scale collimator jaws have been tested in the facility in experiments such as HRMT9, where the aim was to test

three different impact scenarios on an LHC collimation jaw [20–22]. The jaw was subject to an intensity of one LHC bunch at 7 TeV, after which further impacts followed in order to determine the onset of plastic damage. The final test aimed at determining the point at which the jaw, its housing, and the cooling pipes are all damaged extensively. In the HRMT14 experiment, performed in 2012 [23], specimens with uncomplicated geometries were tested to benchmark finite element analysis (FEA) results obtained from analyses conducted with numerical codes including ansys [24] and autodyn [25].

The HRMT36 "MultiMat" experiment [26,27] was conducted in October 2017 at the HiRadMat facility. Building on the experience gathered in previous experiments [23,28], the experiment was intended to offer a reusable test bench to test novel high-performance materials for use in BIDs [29,30]. The experiment tested 18 different materials under a variety of impact scenarios, which provoke a variety of mechanical responses. Centered impacts, for example, result in a longitudinal response, while offset impacts provoke a flexural response. These impact scenarios lead to the generation of a variety of signals, each having distinctive timescales which can be used to decouple the measured waveforms. The main time frames of interest include the rise time, associated with the duration of impact, which is generally in the order of 10 μs, followed by the generation of longitudinal waves with a distinct trapezoidal shape, with a time period in the order of 100 μs. For impacts with transverse offsets, bending oscillations are additionally excited. These have a typical period of around 1 ms [26,31–33].

II. MODELLING COMPOSITES WITH DISPERSED SPHERICAL INCLUSIONS

A. Analytical methods

One of the fundamental problems of mixture theory is the determination of gross material properties from those of its respective constituents. For simplicity's sake, one can consider the propagation of one-dimensional elastic waves in a two-phase elastic material composed of the matrix and rigid spherical inclusions. The average static material properties for such a two-phase elastic material were found by Hashin [34], perhaps most famous for his publication on failure criteria for unidirectional fiber composites [35]. Hashin developed a system to compute the elastic properties, thermal expansion, and strength of composite materials for military and aerospace applications. However, the calculated average modulus was limited to low-frequency wave applications, and such a method is not ideal for the determination of the dispersive effects of waves in inhomogeneous media. Dynamic effects in elastic fiber composites, i.e., layered materials or dispersed fibers, have also been researched by Herrmann and Achenbach [36], who studied wave propagation in the layered direction. While dispersion effects were observed for harmonic waves, the study did not observe any wave attenuation. This was believed to be a result of the periodic nature of layering, as well as what is referred to as the *boundedness* of the body in the direction normal to the wave propagation direction, which results in the confinement of energy.

Micropolar elasticity theories have also been formulated, attempting to incorporate local motions of structured solids through the inclusion of additional constitutive constants. While such theories are able to provide a certain level of consistency and rigor, the additional constants cannot be completely determined from the material properties of the material constituents [37].

The topic of wave propagation in composite materials having dispersed spherical inclusions was studied extensively by Moon and Mow [38], who built on previous solutions for the scattering of elastic compressional waves from rigid inclusions in elastic media [39,40]. The work describes the problem in a number of steps: the general motion of a rigid inclusion, a homogenized model of an elastic mixture, and wave propagation in such a material. Pao and Mow's solution for the equation of motion for a spherical inclusion takes the form of a damped oscillator with memory, similar to a homogeneous viscoelastic spring [39]. This solution, and its implications for wave scattering, is used by Moon and Mow as the basis for the construction of a model of an elastic matrix with randomly distributed spherical inclusions. As discussed in their study, while in periodic inclusion distributions, the scattered waves will either reinforce or cancel each other in certain patterns, forming cutoff bands in the frequency spectrum, this is not necessarily the case in a stochastic medium. Instead, their research aimed to formulate a model that could be used to determine the dispersion and attenuation properties of harmonic longitudinal waves taking into consideration the size of the inclusions, their volumetric distribution in the material, and the elastic properties of the matrix. The study concludes that if the wavelength is large compared to the radius of inclusions, the matrix obeys the wave equation, and the average density of the composite may be used to calculate the resulting wave speed. Otherwise, for wavelengths that are similar in length to the inclusion radius, the material will be both dispersive and dissipative.

The implication of dispersion is that the wave velocity depends on the frequency of vibration. Given that pulsed waves are composed of a spectrum of frequencies, the propagation of such a pulse in a dispersive medium results in spreading, with each frequency component traveling at its own phase velocity. Pao and Mow's model allows for the prediction of the damping time constant for longitudinal motion by considering the thickness and material properties of the matrix, the inclusion density, and the inclusion size.

As detailed, attenuation is the measure of the energy loss of propagating acoustic waves. This is a result of the fact that most media are viscous and nonideal. This thus implies

that there is thermal consumption of energy as an acoustic wave travels through the material, as a result of the medium's viscosity. For an inhomogeneous medium such as CuCD, acoustic scattering additionally contributes to the reduction in acoustic energy [41–43]. The acoustic attenuation coefficient for various porous and viscoelastic materials can be expressed in terms of frequency as a power law:

$$P(x+\Delta x) = P(x)e^{-\alpha(\omega)\Delta x}, \qquad \alpha(\omega) = \alpha_0\omega^{\eta}, \quad (1)$$

where P is the pressure, Δx is the wave propagation distance, ω is the angular frequency, $\alpha(\omega)$ is the attenuation coefficient, α_0 is a frequency-dependent constant, and η is a material parameter obtained by fitting experimental data, ranging from 0 to 2 [44–46]. η is equal to 2 for many metals, crystalline materials, and water, i.e., they are frequency-squared dependent. For viscoelastic materials, this value is generally less than 2—for example, for rock and soil η is roughly equal to 1 [47,48]. In the case of porous and dispersed-particle composites, one could additionally add an exponent considering the wavelength of the propagating wave, depending on its length relative to the porosities or dispersed particles.

B. Numerical methods

In FEA, composite materials are generally modeled by performing experimental testing to determine the global (i.e., equivalent homogeneous) material properties, which can be both costly and time consuming. The numerical simulation of complete composite structures is particularly challenging due to the different length scales involved, with the composite structure usually being much smaller than the actual component. In theory, FEA could be used to simulate such a system on all scales, however, this is not computationally practical, since it requires an incredibly large number of elements and contact points. Such multiscale simulations, or fully coupled numerical analyses, model all dimension ranges of the material's structure, i.e., there is a separate microscopic FEA for each integration point on a macroscopic level [49].

The issue of multiscale simulations being so computationally expensive is solved through the process of homogenization, where material properties of the different constituents making up the composite are averaged to obtain homogenized material data which can then be used to simulate the structure on a macroscopic scale. Homogenization can be done through an analytical approach, as previously described, using methods such as the rule of mixtures or mean-field homogenization [50]. Numerically, solutions have been proposed to determine more accurate homogenized material properties of composites by considering the material properties of representative elements of the material structure [51]. In such simulations, a single preprocessing step is performed, which allows for the calculation of homogenized material data, which is then used to simulate the material on a macroscopic level. This can only be done if there is significant scale separation, that is, the macroscale structure must be significantly larger than the microscale [52]. The composite material is assumed to have a representative microscale structure, referred to as a representative volume element (RVE), which is still large enough to exhibit the material's macroscopic properties. The RVE can be described as a sample of a heterogeneous material which is typical of the whole mixture on average, and one that represents a composite statistically [53,54]. Thus, the volume should include a sample of all microstructural inhomogeneities of the composite material, such as inclusions, voids, and fibers. In general, the required size for an RVE increases with an increase in the mismatch in material properties between the different constituents.

For periodic materials, an RVE can be identified as a unit cell that repeats itself in all directions, as shown in Fig. 1. For nonperiodic materials, a more complex approach needs to be adopted in order to determine a large enough volume

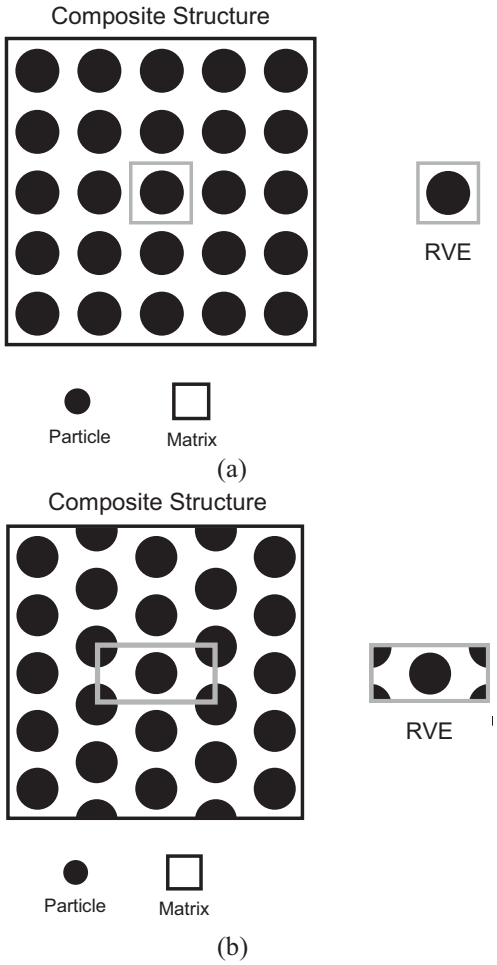

FIG. 1. Representative volume element for a periodic composite composed of a matrix with spheroidal particles organized in a square array (a) and in a hexagonal array (b).

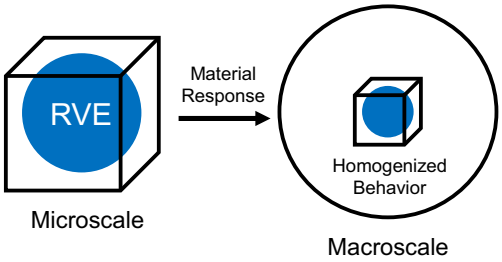

FIG. 2. Representative volume element of a simple periodic composite in the microscale, from which the material response is determined to compute the macroscopic homogenized behavior of the material.

where any further changes to the representative element do not change the macroscopic properties significantly [55]. Once the RVE is modeled, the material properties of the constituent materials can be defined, and the geometry can be meshed for FEA. The RVE is subsequently exposed to a number of macroscopic load cases, which are followed by the calculation of the structural response of the structure. This allows one to calculate the homogenized material data of the material, as visualized in Fig. 2.

C. Wave attenuation effects in CuCD

Wave attenuation in CuCD is a topic that has not been studied extensively in the context of particle accelerator technology and wave propagation induced by particle beam impacts [2]. In the HRMT23 experiment conducted at CERN's HiRadMat facility, an accidental scenario equivalent to an HL-LHC asynchronous beam dump was tested on a CuCD absorber composed of ten 10 cm blocks in series, for a total length of 1 m [2,56]. The thermomechanical state of the absorber was also modeled in ansys® Academic Research Mechanical, Release 18.1 [24], along with additional components such as the clamping system and related pretension, Glidcop housing, and cooling pipes. In the study, two material models were tested, one purely elastic model and an elastoplastic model. The elastic model was observed to drastically overestimate the dynamic strain values measured experimentally, while the elastoplastic model provided a better fit with experimental data. However, the experimentally measured strain signal was observed to quickly decay following a few oscillations, contrasting with the wave propagation in the numerical elastoplastic model, where stress waves decayed in amplitude down to the elastic limit, following which no further energy dissipation occurred. One should also note that this analysis was extended to include modeling of the collimator jaw casing and clamping. The inclusion of the casing and clamping system was found to have little effect on the reduction in strain amplitude with time, reinforcing the idea that the rapid decay in amplitude was not caused by the introduction of frictional contacts with the surrounding structure, but rather due to internal material effects. As discussed in the study, Kolsky [57] used the general term "internal friction" to refer to such dissipative phenomena in materials.

On a mesoscopic level, CuCD has a highly inhomogeneous structure which is composed of diamond particles of approximately 100 μm in diameter, embedded in the copper matrix. A material's shock impedance, found by multiplying the density by the speed of sound in the material, is a measure of the interaction between shock waves and a material's interface. Due to the material's high speed of sound, the shock impedance for diamond is approximately 2 times more than that of copper (61.8 vs 33.8 MPa s m^{-1} in the case of an elastic wave in uniaxial conditions) [2]. Assuming that the wavelength of the traveling wave is small compared to the diamond particles, the relative amplitude of transmitted and reflected waves traveling through a copper-diamond interface can be calculated. The effects of this particle impedance mismatch have been previously studied by modeling in 2D an infinitely long bar submitted to a sinusoidal excitation in a transverse direction [58]. Three main models were considered, namely a mesoscale model with polygonal diamonds in a copper matrix, and two homogeneous CuCD models with a purely elastic and a viscoelastic material model. The model was restricted to diamonds occupying 30% of the total volume to minimize computation time, the diamond particles were scaled to 2 mm in width, and the sinusoidal excitation had a wavelength in the order of 7 mm for a pulse length of 2 μs. The mesoscale model showed strong dispersion in the signal as the wave progressed through the material, as a result of the continuous wave-particle interaction at the copper-diamond interface. This was not captured in the homogeneous elastic model, which showed only a slight decay as a result of dispersive phenomena. The homogeneous viscoelastic model, being time dependent, showed a combination of both dispersion and dissipation and consequently exhibited a larger amplitude decay compared to the elastic model. A similar analysis was conducted with a pulse length of 10 μs and consequently a scaled wavelength in the order of 35 mm. For the mesoscale model, this resulted in less dissipative effects due to particle-wave interactions. In this case, the viscoelastic model was closer to the mesoscale model in terms of the modeled amplitude decay.

It is interesting to note that, despite the fact that signal-damping effects seem to be mostly evident in cases where wavelengths are close to the diamond particle diameter, the dominating frequencies in BIDs are a result of the structure's geometry, which amplifies frequencies that correspond to the block dimensions. In truth, the harmonic response is a result of a combination of factors, one of which is indeed the geometry. The beam parameters, most importantly the pulse duration, determine the input spectrum to which the rod is subjected to, which theoretically includes an infinite number of frequencies.

III. MESOSCALE MODELING OF CuCD

Building on the previous studies on mesoscale effects in material composites [32], this work aims to better understand how the mesoscopic structure of the CuCD RHP3434 grade tested in the MultiMat experiment affects the dynamic response of the material. In the thermomechanical simulations carried out in the referenced study, the material was treated as being homogeneous in nature, and the material model was built by considering data collected from standard mechanical tests that represent the macroscopic material behavior. In most scenarios, this results in acceptable calculations that closely match experimental measurements [27,33,59,60]. As explained, in dynamic scenarios, especially in cases where the wavelength of propagating waves is similar to the diamond particle diameter in the composite, the inhomogeneous nature of the material is believed to induce significant disparities between experimental data and results achieved with a homogeneous model, even when plasticity is included.

The CuCD grade considered in this study and tested in the MultiMat experiment, referred to as CuCD RHP3434, developed by RHP-Technology [14], consists of a 50-50 volume percentage of copper matrix and diamond particles, hot pressed in a spark plasma sintering process. The mixture also includes a small percentage of carbide-forming binding elements, which aid in binding the diamond particles with the copper matrix. The material has a measured porosity of approximately 8%, calculated by considering the ideal density of the material mixture and the measured density. The diamond particles range between 40 and 200 μm in size.

Several numerical models were considered to analyze the mesoscale behavior of the material, and how this compares to homogeneous material models presented in this study. As a starting point, a 1 mm by 0.5 mm specimen was modeled in 2D. The model assumes an infinitely long rod (i.e., plane strain) subjected to an external force on one of its shorter sides. A schematic of homogeneous and mesoscale models adopted is shown in Fig. 3. The mesoscale model is composed of a 50-50 distribution between the copper matrix and the dispersed circular diamond particles, which again have diameters ranging from 40 to 200 μm. The rod is free to move, bar for a symmetry line on the lower edge which restricts vertical movement. An external impact with a rectangular pulse and an amplitude of 100 N is applied to the left side of the model, for a period of 20 ns. Three material models were initially tested, namely a purely elastic homogeneous model, an elastoplastic homogeneous model, utilizing material data from a thermomechanical characterization campaign on CuCD conducted by the authors [32], and a mesoscale model with relevant elastic constituent data for the copper and diamond. A summary of structural material properties at room temperature used for the CuCD homogeneous elastic model, as well as the constituent material data for diamond and copper used in the mesoscale model, are shown in Table I.

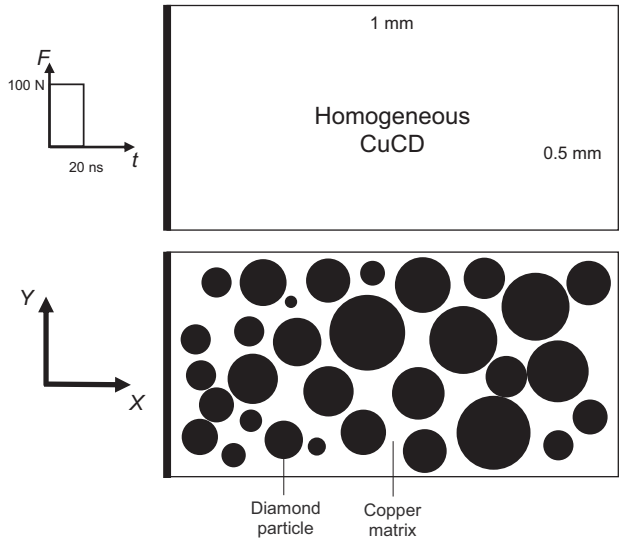

FIG. 3. Homogeneous CuCD geometry (top) and mesoscale copper-diamond geometry (bottom). A force of 100 N was applied in the x-direction to the left side of each model with a rectangular pulse duration of 20 ns.

The resultant stress wave traveling through each specimen can be observed by considering the stress along the centerline at different time points, as shown in Fig. 4. A comparative analysis was conducted on the three models to evaluate the ability of the homogeneous models to accurately replicate the mesoscopic behavior of CuCD.

TABLE I. Elastic material properties for the modeling of an internal heat generation in CuCD for homogeneous and mesoscale models.

Property	Young's modulus	Poisson's ratio	Density	Coefficient of thermal expansion	Specific heat capacity	Conductivity	Speed of sound
Symbol	E	ν	ρ	CTE	C_p	k	c_0
Units	GPa	-	$\mathrm{kgm^{-3}}$	$10^{-6}\ \mathrm{K^{-1}}$	$\mathrm{Jkg^{-1}\,K^{-1}}$	$\mathrm{Wm^{-1}\,K^{-1}}$	$\mathrm{ms^{-1}}$
CuCD	220	0.248	5700	6.7	395	537	6200
Pure copper	130	0.3	8900	17	385	398	3800
Carbon (Diamond)	1143	0.0691	3530	1	520	1000	18000

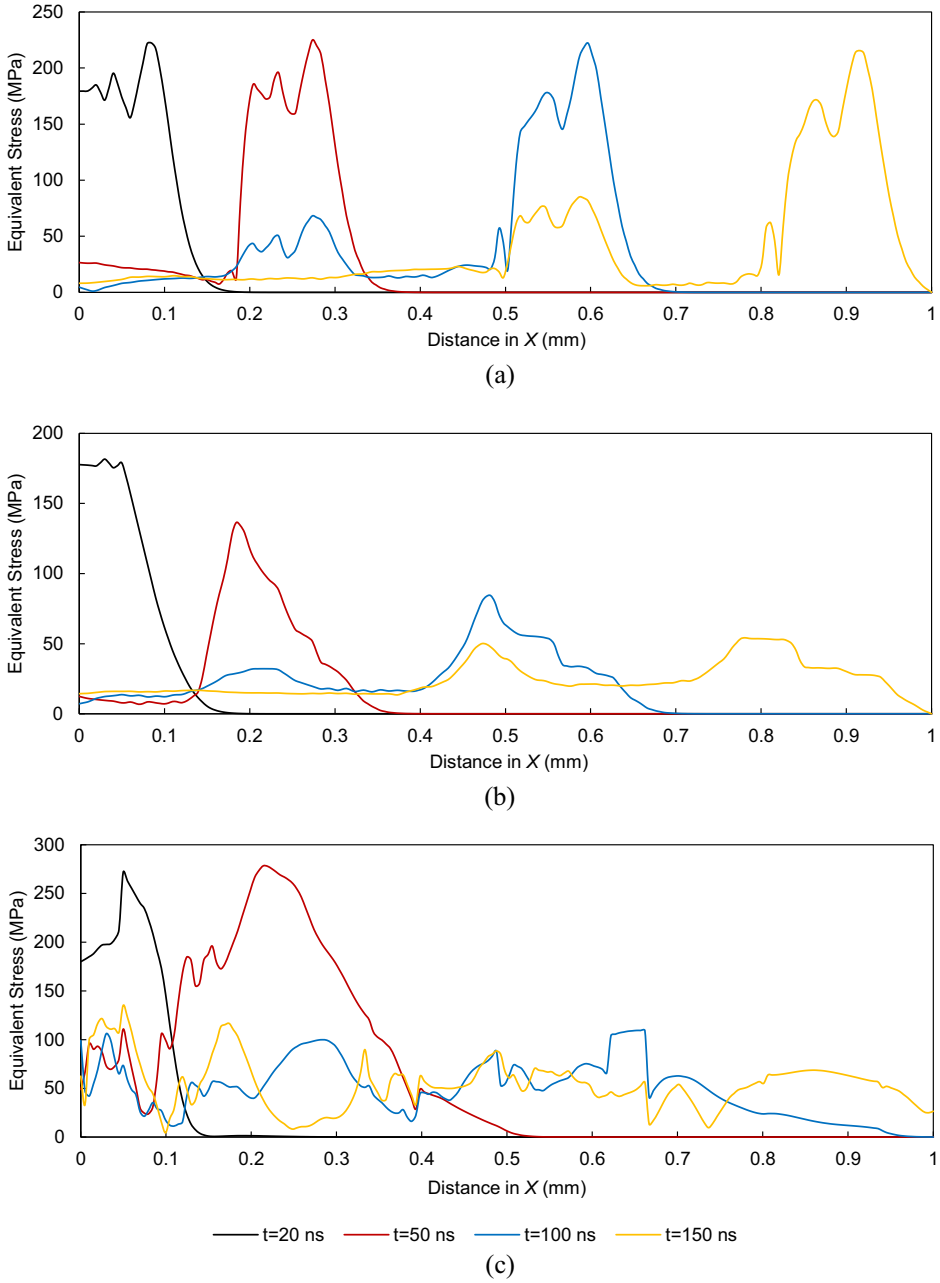

FIG. 4. Stress wave with 20 ns pulse duration traveling through homogeneous elastic (a), homogeneous elastoplastic (b), and mesoscale CuCD (c) specimens.

The mesoscale structure of CuCD, modeled with elastic constituents, can be seen to result in a significant decay in the stress wave. This can be attributed to signal dispersion caused by the continuous reflection of the wave at the copper-diamond interface, which is a result of the wavelength being in the same range as the size of the diamond particles. Considering the speed of sound in CuCD (approximately 6200 ms^{-1}), the wavelength of a 20-ns pulse is in the order of 120 μm.

The homogeneous elastic model fails to capture the significant dispersive effects, and there is only a very slight decay in the propagating signal. The waveform can be seen to retain its trapezoidal shape, wavelength, and amplitude as it travels through the material, in contrast with what is seen in the mesoscale model results. In the 130 ns after impact (i.e., between the 20 and 150 ns observation points), the wave decays approximately 2% in terms of maximum amplitude.

On the other hand, the homogeneous elastoplastic model [32] introduces a high degree of dissipation as a result of its plasticity. This is observed in the stress wave traveling through the material, which decays heavily as it

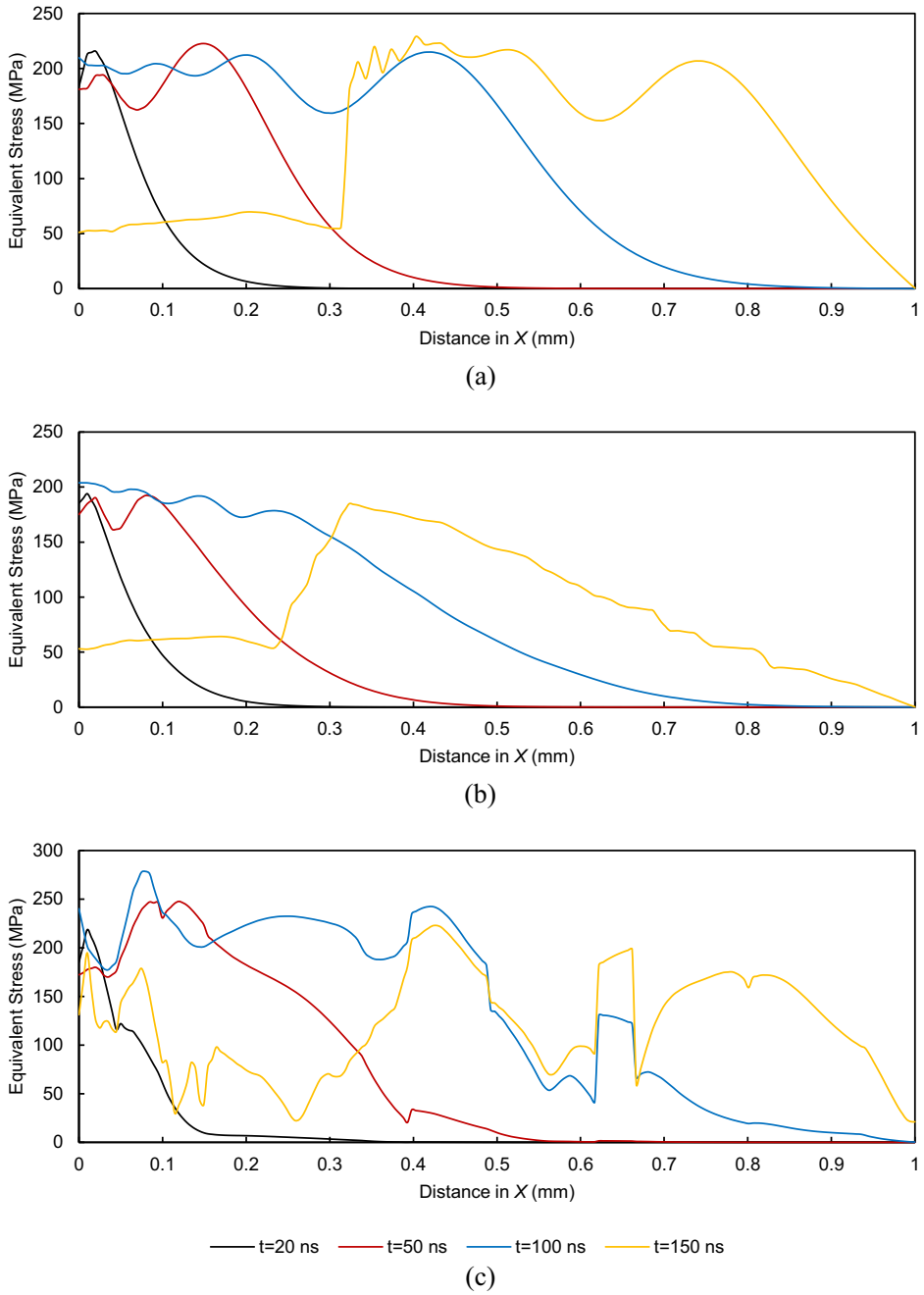

FIG. 5. Stress wave with 100-ns pulse duration traveling through homogeneous elastic (a), homogeneous elastoplastic (b), and mesoscale CuCD (c) specimens.

traverses the length of the specimen, emulating the stress wave traveling through the material's actual internal structure. In this case, the maximum equivalent stress decreases by 70% when comparing the conditions immediately after impact with the wave after 150 ns, similar to the 74% decay in the wave traveling through the mesoscale sample. However, one can note that the stress distribution and maximum stresses experienced in the different model specimens vary significantly. This can be attributed to the fact that the copper and diamond constituents in the mesoscale model have significantly different properties, a characteristic that is not captured in homogeneous models.

A longer pulse, with a period of 100 ns and a wavelength in the order of 600 μm was modeled similarly, the results of which are shown in Fig. 5. In this case, there is a less pronounced decay in the signal from the mesoscale model as the wavelength is significantly larger than the diamond particles, and instead approaches the dimensions of the modeled specimen.

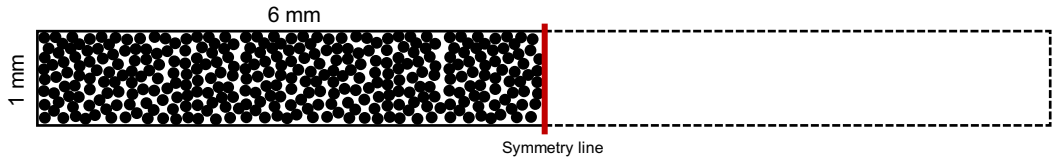

FIG. 6. Mesoscale models adopted for the modeling of internal heat generation and its effects.

In fact, in this scenario, wave dispersion is much more prominent in all three models as the wave interacts with the defined boundaries.

Since the application of interest for CuCD in this work is related to BIDs, where the material is subjected to sudden increases in internal temperature as a result of the interaction between subatomic particles and the material, an attempt was made to model such a scenario on a mesoscale level.

Similarly to the structural analyses described above, two main types of models were tested, namely a homogeneous model and a mesoscale model. A specimen measuring 6 mm by 1 mm, with symmetry for a total effective length of 12 mm, was once again modeled in 2D, as shown in Fig. 6. The mesoscale model consisted of a copper matrix with 375 diamond particles each having a diameter of 100 μm, for a 50-50 percentage area distribution. The same material models described in the previous analysis (shown in Table I) were utilized. Note that for a length of 12 mm, the fundamental period for vibrations for CuCD is $t_L = 2L/c_0 = 3.9$ μs, where L is the length and c_o is the speed of sound (approximately 6200 m/s for CuCD).

The simulation, conducted in ansys® Academic Research Mechanical, Release 18.1, comprised a sequentially coupled thermomechanical analysis, starting with a 2D thermal analysis that consisted of an internal heat generation throughout the specimen, aiming to achieve maximum temperatures comparable to those experienced in specimens tested in the MultiMat experiment. This results in a uniform temperature increase in the homogeneous model, but, due to the different thermal properties of copper and diamond, there is a different temperature increase in the two materials. The results from the thermal simulation were applied as a thermal load in a 2D (plane strain) structural analysis of the specimen in a free condition.

Two pulse durations were considered, namely 300 and 20 ns, corresponding to typical energy deposition times tested in the MultiMat experiment for CuCD RHP3434 samples. For the 300-ns shot, an intensity of 10^{15} W/m^3 was applied in the thermal analysis. The 20-ns shot was modeled with a scaled intensity of 1.5×10^{16} W/m^3, resulting in an equal amount of deposited energy for the two scenarios considered. As mentioned, the energy deposition for both scenarios gives an internal temperature similar to that achieved in the MultiMat experiment. For the 300-ns shot, the maximum temperature in the homogeneous model was equal to a uniform 138 °C throughout the geometry. For the mesoscale model, the diamond particles reached a maximum temperature of 185 °C while the copper matrix reached a temperature of 107 °C following the energy deposition (for an average temperature of 146 °C at the end of the energy deposition). These results are in contrast with what would happen in an actual beam impact, where the diamond particles would absorb less

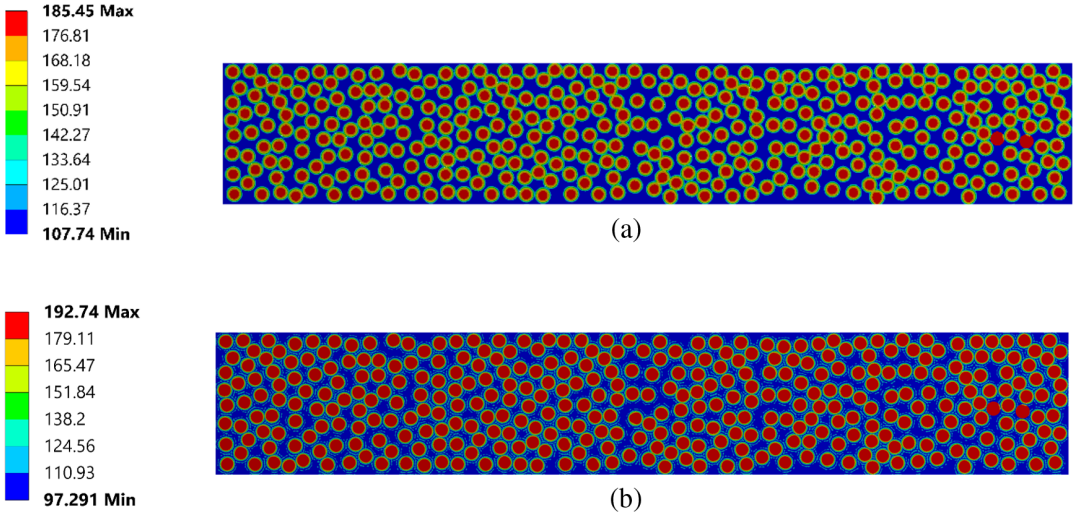

FIG. 7. Temperature reached (in °C) in the mesoscale model at the end of the energy deposition for the two shots considered (a, at 300 ns) and (b, at 20 ns) with total intensity of 10^{15} W/m^3 and 1.5×16^5 W/m^3, respectively.

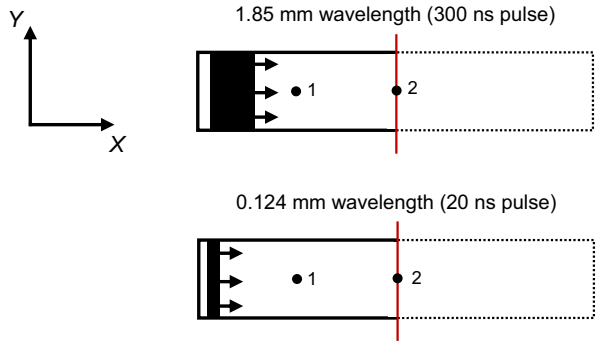

FIG. 8. Position of probe points (1 and 2) on the specimen, along with a representative wavelength and direction of wave travel for 300 and 20 ns pulses (not to scale).

power due to their lower density relative to the copper matrix. Similar results were achieved for the 20-ns shot, with slightly higher maximum temperatures and lower minimum temperatures due to the faster energy deposition (and therefore less time for heat to dissipate throughout the body during the pulse duration). Thermal analysis results at 300 and 20 ns for the two shots considered are shown in Fig. 7.

For the structural analysis, the material model used for the copper matrix was updated to include a bilinear kinematic hardening model for the inclusion of plasticity, with a yield strength of 200 MPa and a tangent modulus of 160 MPa. Four scenarios were thus considered: (i) homogeneous CuCD model with elastic material properties; (ii) homogeneous CuCD model with plasticity (multilinear hardening curve); (iii) mesoscale model with elastic material properties; and (iv) mesoscale model with plasticity in the copper matrix.

The resulting respective expected wavelengths for the two shots (generated from the free ends of the modeled geometry) along with the points on the model at which results of interest were probed, are shown in Fig. 8.

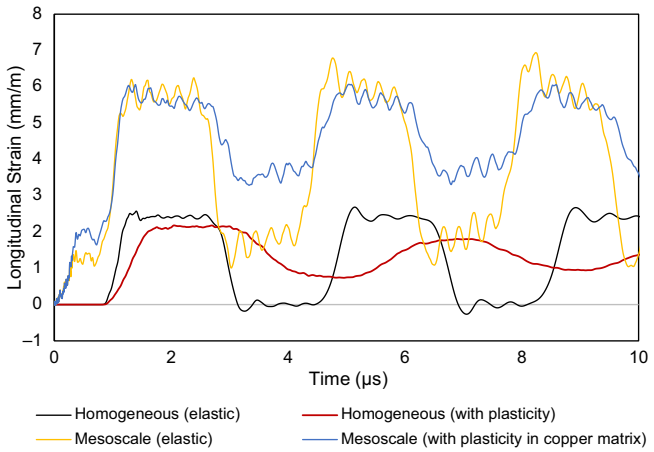

FIG. 9. Longitudinal strain results for the 300-ns shot at the center point of the specimen.

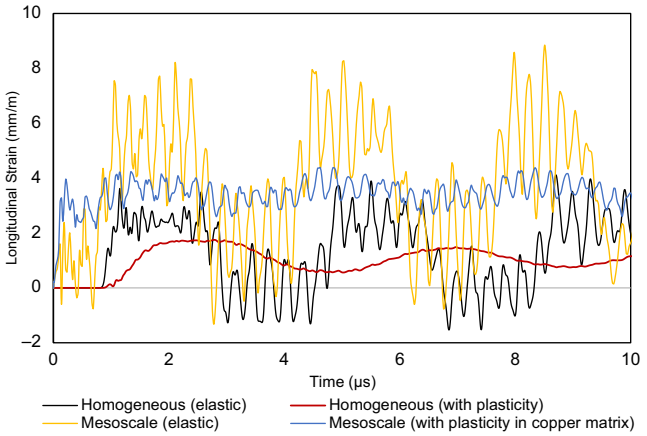

FIG. 10. Longitudinal strain results for the 20-ns shot at the center point of the specimen.

Figures 9 and 10 show the longitudinal strain results probed at the center of the simulated specimen, i.e., at a longitudinal length of 6 mm and a transverse length of 0.5 mm, for the modeled 300 and 20 ns shots, respectively. The figures show results for the four simulated models, namely a homogeneous model with elastic properties, a homogeneous model with the inclusion of elastoplastic properties (the multilinear hardening curve obtained through a four-point bending test), a mesoscale model with 100 μm diamond particles with elastic properties, and a mesoscale model with an elastoplastic model for the copper matrix.

All elastic models can be seen to exhibit very similar frequencies, indicating that the homogeneous model's elastic properties manage to average the material's mesoscale behavior well in terms of wave propagation effects. The inclusion of plasticity in the copper matrix of the mesoscale structure results in a significant decrease in the amplitude of the propagating wave when compared to the mesoscopic model with elastic properties.

For the 300-ns shot, the results from the mesoscale model with plasticity in the copper matrix (blue) are somewhat comparable to results from the homogeneous elastic model (black). Despite the clear difference in total strain between the two results, with the mesoscale model exhibiting much larger strains, in both cases, the dynamic components have similar amplitudes which are maintained for various oscillations without significant decay. This is in contrast with what is observed in the homogeneous elastoplastic model, where the energy dissipation introduced as a result of the included plasticity gives an observable decay in wave amplitude, as well as a significant reduction in frequency due to the change in stiffness.

For the 20-ns shot, one can observe a significant increase in high-frequency content for all modeled scenarios. These are observed in both the mesoscopic models, as well as the homogeneous elastic model, and can therefore be assumed to be a result of wave-boundary interactions and Poisson

effects, rather than due to the interaction of the pulse with diamond particles of approximately the same size as the wavelength. Considering this, the results for the mesoscale model with plasticity in the copper matrix and the homogeneous elastoplastic model shown in Fig. 10 are comparable in terms of their dynamic features (namely wave amplitude) and decay rate.

IV. CONCLUSIONS

In this study, the simulation of wave propagation effects in a stochastic CuCD composite was presented, aiming to compare and contrast differences between a model considering the mesoscale structure of the composite and another trying to capture the material behavior through a homogenized model. The homogenized model was built through standardized material characterization techniques, including a four-point bending test to determine the stress-strain relationship of the material. The mesoscale model was built by considering the material data for the two constituents making up the composites.

A case study was modeled in 2D by considering a small, slender specimen in plane strain. The size considered was based on computational limitations, and the chosen geometry aimed to represent the slender nature of BIDs. Two scenarios were considered for each model, the first consisting of an external impact on one side of the modeled specimen, which results in a stress wave propagating through the material. The second scenario consisted of a thermomechanical simulation where the specimen was, similarly, dynamically loaded with a thermal pulse, with an energy deposition time in the order of nanoseconds, which also results in a dynamic structural response. The two cases successfully modeled the propagation of the stress wave throughout the different models tested.

The wavelength of disturbances traveling through the material can be seen to have a significant effect on results. In the study, two pulse durations were considered, namely 20 and 300 ns. These correspond to typical impact times of shots tested in experiments such as the HRMT36 MultiMat experiment. For CuCD, such pulse durations result in wavelengths of approximately 0.12 and 1.85 mm, respectively. Wave-particle interaction was observed to increase substantially as the wavelength approaches the size of the diamond particles modeled, which for the CuCD grade is in the order of 0.1 mm.

To conclude, the homogeneous model adopted for CuCD can be seen to produce results that are qualitatively similar to the mesoscale model. In some scenarios, the homogeneous models managed to adequately capture wave propagation effects within the material, especially with the inclusion of the plasticity behavior of the material. Model limitations are particularly apparent in the case of wavelengths that approach the particle size of diamond particles. Additionally, computed total strains were at some points observed to be 2 to 3 times higher for the mesoscale models when compared to their homogeneous counterparts. Despite this, the dynamic components were much still comparable in terms of amplitude and observed frequencies.

Given the computational requirements of a full-scale, 3D mesoscale model, such an analysis would not be feasible to model a scenario such as a whole LHC tertiary collimator or a specimen of similar dimensions to those tested in the HRMT36 experiment. For the 6 mm $\times$ 1 mm 2D model considered in this study, the computation time for the mesoscale models was approximately 2 orders of magnitude higher than that for the homogeneous models, with the mesoscale model requiring a significantly large number of elements and contact points between the copper matrix and modeled diamond particles.

Further study can be conducted on the simulation of nonuniform energy distributions built on a homogeneous model, such as those generated in fluka [61], compared with an energy deposition that considers the different energy absorption characteristics of the copper matrix and the diamond particles. This would show whether energy density maps built on homogeneous models can be effective in modeling the mesoscale nature of the material. Finally, to avoid wave-boundary interactions distorting results, future studies on the subject would benefit from modeling wave propagation in a semi-infinite body where the specimen dimensions are much larger than the modeled wavelengths.

ACKNOWLEDGMENTS

This project has received funding from the European Union's Horizon 2020 Research and Innovation program under Grant Agreement No. 730871.

[1] K. Sobczyk, *Stochastic wave propagation* (Elsevier, Amsterdam, New York, 1985) [accessed July 09, 2020 [Online], available at http://site.ebrary.com/id/10675894.

[2] F. Carra, Thermomechanical response of advanced materials under quasi instantaneous heating, Ph.D. thesis, Politecnico di Torino, Italy, 2017.

[3] A. S. Barnard, *The Diamond Formula: Diamond Synthesis—A Gemmological Perspective* (NAG Press, London, 2008).

[4] S. Kidalov and F. Shakhov, Thermal conductivity of diamond composites, Materials **2**, 2467 (2009).

[5] K. Chu, Z. Liu, C. Jia, H. Chen, X. Liang, W. Gao, W. Tian, and H. Guo, Thermal conductivity of SPS consolidated Cu/diamond composites with Cr-coated diamond particles, J. Alloys Compd. **490**, 453 (2010).

[6] Th. Schubert, B. Trindade, T. Weißgärber, and B. Kieback, Interfacial design of Cu-based composites prepared by powder metallurgy for heat sink applications, Mater. Sci. Eng. A **475**, 39 (2008).

[7] K. Yoshida and H. Morigami, Thermal properties of diamond/copper composite material, Microelectron. Reliab. **44**, 303 (2004).

[8] Y. Zhang, H. L. Zhang, J. H. Wu, and X. T. Wang, Enhanced thermal conductivity in copper matrix composites reinforced with titanium-coated diamond particles, Scr. Mater. **65**, 1097 (2011).

[9] H. J. Cho, Y.-J. Kim, and U. Erb, Thermal conductivity of copper-diamond composite materials produced by electrodeposition and the effect of TiC coatings on diamond particles, Composites, Part B **155**, 197 (2018).

[10] P. T. Jochym, K. Parlinski, and M. Sternik, TiC lattice dynamics from *ab initio* calculations, Eur. Phys. J. B **10**, 9 (1999).

[11] R. M. Mazitov, V. A. Semenov, Yu. A. Lebedev, R. R. Mulyukov, G. I. Raab, E. L. Yadrovskii, and V. N. Danilenko, Density of phonon states in nanostructured copper, JETP Lett. **92**, 238 (2010).

[12] J. Xie, S. P. Chen, J. S. Tse, S. de Gironcoli, and S. Baroni, High-pressure thermal expansion, bulk modulus, and phonon structure of diamond, Phys. Rev. B **60**, 9444 (1999).

[13] T. Weißgärber, Copper/diamond composites for heat sink applications, Fraunhofer IFAM (2019), https://www.nanoanalytik.fraunhofer.de/en/library/CS1.html.

[14] RHP-Technology GmbH (2019), http://www.rhp-technology.com/.

[15] M. Kitzmantel, Developments and novelties in thermal management by RHP-technology, in *Proceedings of the EuCARD-2 Workshop on Applications of Thermal Management Materials* (CERN, Geneva, 2015) [online]. Available at http://indico.cern.ch/event/400452/.

[16] A. Bertarelli *et al.*, Novel materials for collimators at LHC and its upgrades, in *Proceedings of HB2014, East Lansing, MI* (2014), pp. 438–442, https://accelconf.web.cern.ch/HB2014/papers/tho4ab03.pdf.

[17] I. Efthymiopoulos *et al.*, HiRadMat: A new irradiation facility for material testing at CERN, in *Proceedings of the 2nd International Particle Accelerator Conference, San Sebastián, Spain* (EPS-AG, Spain, 2011), pp. 1665–1667.

[18] HiRadMat Beam Parameters, CERN official website, https://espace.cern.ch/hiradmat-sps/Wiki%20Pages/Beam%20Parameters.aspx.

[19] High-Radiation to Materials (HiRadMat) Facility of CERN/SPS, CERN official website. https://espace.cern.ch/hiradmat-sps/Wiki%20Pages/Home.aspx.

[20] F. Carra *et al.*, Mechanical engineering and design of novel collimators for HL-LHC, in *Proceedings of the 5th International Particle Accelerator Conference, IPAC2014, Dresden, Germany* (JACoW, Geneva, Switzerland, 2014), 10.18429/JACoW-IPAC 2014-MOPRO116.

[21] A. Bertarelli *et al.*, Permanent deformation of the lhc collimator jaws induced by shock beam impact: An analytical and numerical interpretation, in *Proceedings of the 10th European Particle Accelerator Conference, Edinburgh, Scotland, 2006* (EPS-AG, Edinburgh, Scotland, 2006), p. 3.

[22] M. Cauchi *et al.*, High energy beam impact tests on a LHC tertiary collimator at the CERN high-radiation to materials facility, Phys. Rev. ST Accel. Beams **17**, 021004 (2014).

[23] A. Bertarelli *et al.*, High Energy Tests of Advanced Materials for Beam Intercepting Devices at CERN HiRadMat Facility, p. 5 (2012).

[24] ANSYS, Inc., ansys Mechanical User's Manual—Release 15.0 (2013).

[25] ANSYS, Inc., ansys autodyn User's Manual—Release 15.0 (2013).

[26] F. Carra *et al.*, The "Multimat" experiment at CERN HiRadMat facility: advanced testing of novel materials and instrumentation for HL-LHC collimators, J. Phys. Conf. Ser. **874**, 012001 (2017).

[27] M. Pasquali *et al.*, Dynamic response of advanced materials impacted by particle beams: The MultiMat experiment, J. Dyn. Behav. Mater. **5**, 266 (2019).

[28] A. Bertarelli *et al.*, An experiment to test advanced materials impacted by intense proton pulses at CERN HiRadMat facility, Nucl. Instrum. Methods Phys. Res., Sect. B **308**, 88 (2013).

[29] E. Quaranta, Investigation of collimator materials for the High Luminosity Large Hadron Collider, Ph.D. thesis, Politecnico di Milano, Italy, 2017.

[30] A. Bertarelli, F. Carra, N. Mariani, and S. Bizzaro, Development and testing of novel advanced materials with very high thermal shock resistance, EuCARD-2 Scientific Report No. CERN-ACC-2014-0306, 2014 [accessed February 06, 2018] [Online]. Available at https://cds.cern.ch/record/1973365/files/CERN-ACC-2014-0306.pdf.

[31] A. Bertarelli, Beam-induced damage mechanisms and their calculation, CERN Report No. 0007–8328, 2016 [accessed February 06, 2018] [Online]. Available at https://e-publishing.cern.ch/index.php/CYR/article/view/234.

[32] M. Portelli *et al.*, Thermomechanical characterisation of copper diamond and benchmarking with the MultiMat experiment, Shock Vib. **2021**, 8879400 (2021).

[33] M. Portelli, A. Bertarelli, F. Carra, M. Pasquali, N. Sammut, and P. Mollicone, Numerical and experimental benchmarking of the dynamic response of SiC and TZM specimens in the MultiMat experiment, Mech. Mater. **138**, 103169 (2019).

[34] Z. Hashin, Theory of mechanical behavior of heterogeneous media, University of Pennsylvania, Technical Report (1963) [accessed July 09, 2020]. [Online]. Available: https://apps.dtic.mil/sti/pdfs/AD0412503.pdf.

[35] Z. Hashin, Failure criteria for unidirectional fiber composites, J. Appl. Mech. **47**, 329 (1980).

[36] G. Herrmann and J. Achenbach, On dynamic theories of fiber composites, in *Proceedings of the 8th Structural Dynamics and Materials Conference* (Palm Springs, CA, 1967).

[37] A. C. Eringen, Linear theory of Micropolar Elasticity, Office of Naval Research US, AD664271 (1967).

[38] F. C. Moon and C. C. Mow, Wave propagation in a composite material containing dispersed rigid spherical inclusions, U.S. Air Force Project RAND Report No. RM-6139-PR, 1970.

[39] Y. Pao and C. C. Mow, Scattering of plane compressional waves by a spherical obstacle, J. Appl. Phys. **34**, 493 (1963).

[40] C. C. Mow, On the effects of stress-wave diffraction on ground-shock measurements: Part I, The Rand Corporation Report No. RM-4341-PR, 1965.

[41] Y. Chen and J. Ma, Random noise attenuation by f-x empirical-mode decomposition predictive filtering, Geophysics **79**, V81 (2014).
[42] Y. Chen, G. Zhang, S. Gan, and C. Zhang, Enhancing seismic reflections using empirical mode decomposition in the flattened domain, J. Appl. Geophys. **119**, 99 (2015).
[43] Y. Chen, Dip-separated structural filtering using seislet transform and adaptive empirical mode decomposition based dip filter, Geophys. J. Int. **206**, 457 (2016).
[44] T. L. Szabo and J. Wu, A model for longitudinal and shear wave propagation in viscoelastic media, J. Acoust. Soc. Am. **107**, 2437 (2000).
[45] T. L. Szabo, Time domain wave equations for lossy media obeying a frequency power law, J. Acoust. Soc. Am. **96**, 491 (1994).
[46] W. Chen and S. Holm, Modified Szabo's wave equation models for lossy media obeying frequency power law, J. Acoust. Soc. Am. **114**, 2570 (2003).
[47] J. M. Carcione, F. Cavallini, F. Mainardi, and A. Hanyga, Time-domain modeling of constant-Q seismic waves using fractional derivatives, Pure Appl. Geophys. **159**, 1719 (2002).
[48] W. Chen and S. Holm, Fractional Laplacian time-space models for linear and nonlinear lossy media exhibiting arbitrary frequency power-law dependency, J. Acoust. Soc. Am. **115**, 1424 (2004).
[49] V. Kouznetsova, Computational homogenization for the multi-scale analysis of multi-phase materials, Ph.D thesis, Technische Universiteit Eindhoven, Eindhoven, 2002.
[50] R. Younes, A. Hallal, F. Fardoun, and F. Hajj, Comparative review study on elastic properties modeling for unidirectional composite materials, in *Composites and their Properties*, edited by N. Hu (IntechOpen, 2012), ISBN 978-953-51-0711-8, 10.5772/50362.
[51] F. Pavia, How to simulate and design the microstructures of composites and other complex materials, https://www.ansys.com/blog/how-to-simulate-microstructures-composites#:~:text=Ansys%20Material%20Designer%2C%20available%20in,of%20complex%20materials%20and%20composites [accessed July 16, 2020].
[52] M. G. D. Geers, V. G. Kouznetsova, and W. A. M. Brekelmans, Multi-scale computational homogenization: Trends and challenges, J. Comput. Appl. Math. **234**, 2175 (2010).
[53] R. Hill, Elastic properties of reinforced solids: Some theoretical principles, J. Mech. Phys. Solids **11**, 357 (1963).
[54] S. L. Omairey, P. D. Dunning, and S. Sriramula, Development of an ABAQUS plugin tool for periodic RVE homogenisation, Eng. Comput. **35**, 567 (2019).
[55] S. Li, L. F. C. Jeanmeure, and Q. Pan, A composite material characterisation tool: UnitCells, J. Eng. Math. **95**, 279 (2015).
[56] E. Quaranta *et al.*, Towards optimum material choices for HL-LHC collimator upgrade, *Proceedings of IPAC2016, Busan, Korea* (2016), pp. 2498–2501, https://accelconf.web.cern.ch/ipac2016/papers/wepmw031.pdf.
[57] H. Kolsky, *Stress Waves in Solids*, 2nd ed. (Dover Publications, New York, 1963).
[58] F. Carra, Numerical analyses of novel materials under quasi-instantaneous heat deposition, in *Thermomechanical Response of Advanced Materials under Quasi Instantaneous Heating* (Politecnico di Torino, Italy, 2017), pp. 219–224, https://www.researchgate.net/publication/325711142_Thermomechanical_Response_of_Advanced_Materials_under_Quasi-Instantaneous_Heating#fullTextFileContent.
[59] A. Bertarelli *et al.*, Dynamic testing and characterization of advanced materials in a new experiment at CERN HiRadMat Facility, J. Phys. Conf. Ser. **1067**, 082021 (2018).
[60] M. Portelli, A. Bertarelli, F. Carra, L. K. Mettler, P. Mollicone, and N. Sammut, Numerical simulation of long rods impacted by particle beams, Phys. Rev. Accel. Beams **21**, 063501 (2018).
[61] A. Ferrari, P. R. Sala, A. Fassò, and J. Ranft, *FLUKA: A multi-particle transport code* (CERN, Geneva, 2005).